CHEMISTRY OF MATERIALS
Cite This: Chem. Mater. 2019, 31, 4228−4233
Article
pubs.acs.org/cm

Mn Cations Control Electronic Transport in Spinel $Co_xMn_{3-x}O_4$ Nanoparticles

Anuj Bhargava,[†] Cindy Y. Chen,[†] Kapil Dhaka,[§] Yuan Yao,[†] Andrew Nelson,[†] Kenneth D. Finkelstein,[‡] Christopher J. Pollock,[‡] Maytal Caspary Toroker,[∥,§] and Richard D. Robinson*[,†]

[†]Department of Materials Science and Engineering and [‡]Cornell High Energy Synchrotron Source (CHESS), Cornell University, Ithaca, New York 14853, United States

[§]Department of Materials Science and Engineering and [∥]The Nancy and Stephen Grand Technion Energy Program, Technion - Israel Institute of Technology, Haifa, 3200003, Israel

Supporting Information

ABSTRACT: Understanding the mechanisms of charge transport in ternary and higher order spinels would enable design principles for enhancing their electronic and electrochemical properties for energy applications. Here we investigate the ternary $Co_xMn_{3-x}O_4$ spinel system and determine the relationship between electronic properties and cation site occupation, based on the octahedral site, donor−acceptor formalization introduced in the polaron hopping model. We employ synchrotron X-ray emission spectroscopy to characterize the donor−acceptor cation pairs in the lattice. We find that the stochiometric volcano trend in electronic conductivity correlates well with the concentration of Mn^{4+}/Mn^{3+} hopping pairs, while the concentration of Mn^{3+}/Mn^{2+} pairs is unchanged with stoichiometry. We also find that Co does not directly contribute to conductivity; however, the Co does create configurational disorder that leads to the generation of hopping pairs for Mn at octahedral sites. From these results we conclude that Mn^{4+}/Mn^{3+} pairs are the dominant active species and the origin of the stoichiometry-dependent behavior for polaron charge transport. This work provides a starting point for understanding and optimizing charge transport for higher order spinels.

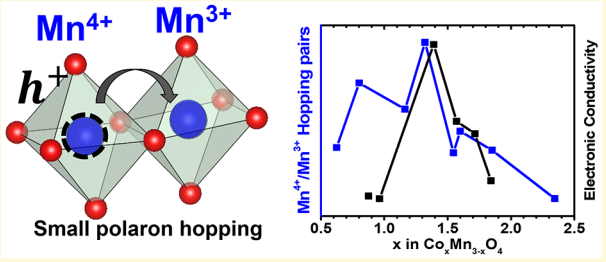

Mixed-valence ternary spinel oxides exhibit electronic and electrochemical properties, such as conductivity and charge-storage capacity, that can be significantly improved relative to those of binary spinel oxides.[1,2] Although it is known that the presence of multiple cation species at different sublattice sites gives rise to enhanced transport properties,[3] the exact nature of this enhancement is still poorly understood. Currently, the polaron hopping model is used to describe charge transport in spinels, wherein the charge carrier receives energy from lattice vibrations and hops from one cation site to another.[1,4] However, the polaron hopping model is only accurate for binary spinels (A_3O_4). Higher order spinels, like ternary spinels having the chemical formula $(A_tB_{1-t})[A_xB_{2-x}]O_4$ (where A and B are metal cations that can occupy tetrahedral (T_d) sites or octahedral [O_h] sites and $0 \le t \le 1$, $0 \le x \le 2$), exhibit configurational variations that are not accounted for in the small polaron hopping model. The configurational variations include different concentrations and oxidation states of cation species at the tetrahedral and octahedral sites and depend on processing conditions and stoichiometry. For instance, at the fixed stoichiometry of $x = 1$ in the $Co_xMn_{3-x}O_4$ system, the average oxidation state and the concentration of Mn cations at octahedral sites have been observed to vary as a function of the synthesis temperature.[5] Furthermore, cation site occupancy can also change with varying degrees of configurational disorder in the nonstoichiometric $Co_xMn_{3-x}O_4$ system. Due to this configurational disorder in the $Co_xMn_{3-x}O_4$ system, the charge carriers could move through several conduction pathways, i.e., charge transfer by polaron hopping could take place between similar cation species (Co to Co or Mn to Mn) or between different cation species (Co to Mn), as mediated by various donor−acceptor pairs (e.g., Mn^{3+}/Mn^{2+} or Mn^{4+}/Mn^{3+}). As a result of the deficient polaron hopping model and the large degree of cation configurational variations in ternary oxides, specifying the fundamental mechanisms of properties such as electronic conduction and electrochemical behavior, is difficult. One of the main limitations holding back more accurate descriptions of charge transport in oxides has been the lack of facile and accessible characterization methods to precisely determine the site occupation of the cations.[6] Another complication in laying out design principles for nanoparticle (NP) oxide systems is the high number of grain boundaries (GB) in assembled films, which requires deconvolving the GB contributions to extract the intrinsic intraparticle (IP) electronic conductivity. Overcoming these

Received: March 26, 2019
Revised: April 28, 2019
Published: April 30, 2019

DOI: 10.1021/acs.chemmater.9b01198
Chem. Mater. 2019, 31, 4228−4233

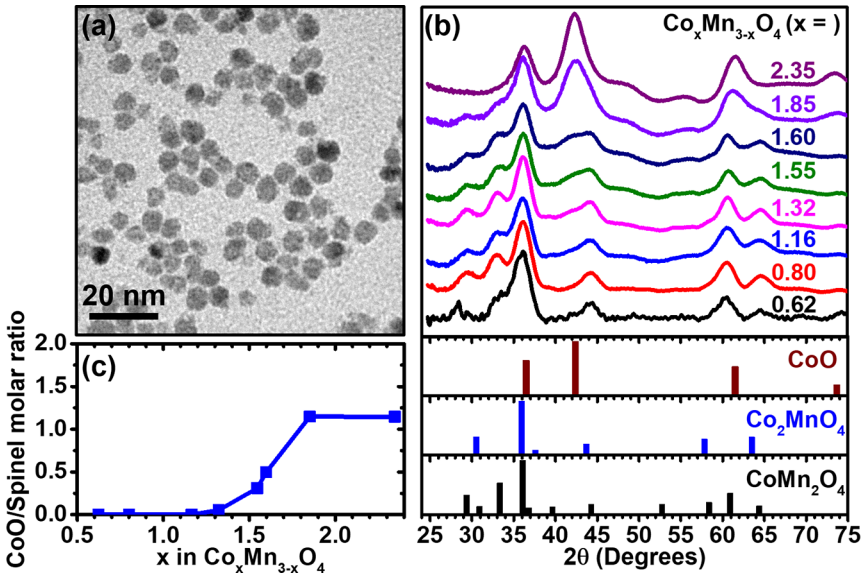

Figure 1. Transmission electron microscopy (TEM) image and synchrotron X-ray diffraction (SXRD) for the characterization of $Co_xMn_{3-x}O_4$ nanoparticles (NPs). (a) TEM image corresponds to the model system $Co_{1.60}Mn_{1.40}O_4$ NPs after oxidation at 200 °C for 4 h. These oxidized NPs are spherically shaped with an average diameter of 5.7 ± 1.0 nm. (b) SXRD of $Co_xMn_{3-x}O_4$ NPs for x = 0.62 to 2.35 (x values are determined from XES). The bar patterns show the reference XRD patterns for $CoMn_2O_4$ (JCPDS: 01-077-0471), Co_2MnO_4 (JCPDS: 01-084-0482), and CoO (JCPDS: 00-48-1719). Note: 2θ scale for SXRD patterns are shifted to match Cu K_α, raw Q-space data is shown in Figure S2. (c) Moles of CoO per mole of spinel $Co_xMn_{3-x}O_4$ as determined from XES analysis.

challenges can lead to a more detailed delineation of the cation site occupancy with the ultimate goal of uncovering the fundamental link between configurational disorder and material properties. With known information on the material properties, we can then adjust the design principles to create better performing energy devices.

In this study, we investigate the spinel $Co_xMn_{3-x}O_4$ NP system, an interesting material with potential for applications such as catalysts and the active material in energy storage devices.[2,5,7−9] We previously showed that the $Co_xMn_{3-x}O_4$ NP system exhibits an anomalous peak in supercapacitor performance at the 1:1 ratio of Co:Mn in $Co_xMn_{3-x}O_4$ NPs.[2] This enhancement was hypothesized to originate from an increased and synergistic concentration of Co and Mn redox couples at the peak stoichiometry. But the conclusion in this study was based on X-ray photoemission spectroscopy (XPS), which was only able to characterize the average concentration of redox pairs and not their corresponding site location. A more recent study reported Mn cations as the activity descriptor for oxygen electrocatalysis in $MnCo_2O_4$, but this work relied on the less-accurate methods of X-ray absorption spectroscopy (XAS), which convolves averages of oxidation state and site location to generalize descriptions of the cations, and the work did not examine the significant influence of the stoichiometric dependent conductivity.[5] To elucidate the fundamental mechanisms, it is necessary to accurately identify the octahedral site cations, because charge is believed to hop through donor−acceptor pairs at octahedral sites,[3] and determine the correlation between active redox couples and properties. In this present work, we address the aforementioned characterization challenges by using X-ray emission spectroscopy (XES) to identify the site occupation of cations and dielectric spectroscopy to extract the intrinsic intraparticle electronic conductivity. Using these methods, we determine the identity of the active redox couples mediating polaron hopping and find that their concentration is positively correlated to the electronic conductivity. Finally, we show from first-principles simulations that the density of states at the conduction band is larger at an intermediate stoichiometry, in agreement with our experiments. This finding indicates that electronic transport in the conduction band could significantly increase overall conductivity, but this contribution is not considered in the current polaron hopping models.

Co−Mn metal NPs were synthesized by the hot injection of organometallic precursors into a solution of surfactants, as described previously.[2,10] The metal NPs were then oxidized in air at 200 °C for 4 h to form spinel oxides. Both the metal and oxidized NPs adopt a spherical morphology with diameters ranging from 3 to 7 nm and with a size distribution of 15% to 25% for each stoichiometry (Figure 1a, Table S1, and Figure S1a−h). The oxidized NPs range in stoichiometry from x = 0.62 to 2.35 in the chemical formula $Co_xMn_{3-x}O_4$, where the value of x is determined using XES as described previously.[10] The phase of the oxide NPs, as characterized by synchrotron X-ray diffraction (SXRD), is a mixture of spinel and CoO phases with progressively more CoO impurity as the Co content increases (Figure 1b and Figure S2). The diffraction peaks for samples x = 0.62 to 1.60 correspond to the spinel phases, while the two highest Co-content samples (x = 1.85 and 2.35) have peaks that are dominated by the CoO impurity (see SI for details). The phase concentration is accurately determined from XES using the $K\beta_{1,3}$ peak and its satellite peak, $K\beta'$ (see SI for details).[10] XES analysis reveals that the CoO impurity is negligible for $x \leq 1.32$, but the impurity concentration increases with increasing Co content in the samples. For the most Co-rich stoichiometries (x = 1.85 and 2.35), a large amount of CoO impurity is present (Figure 1c and Figure S2b). For $x > 2.35$, only the CoO and no spinel Co_3O_4 phase was observed; hence, all samples with $x > 2.35$ are excluded from further analysis. Due to the presence of this impurity, the oxidized NPs are suitably expressed as $Co_xMn_{3-x}O_4 \cdot (CoO)_y$, where $Co_xMn_{3-x}O_4$ represents the

DOI: 10.1021/acs.chemmater.9b01198
Chem. Mater. 2019, 31, 4228−4233

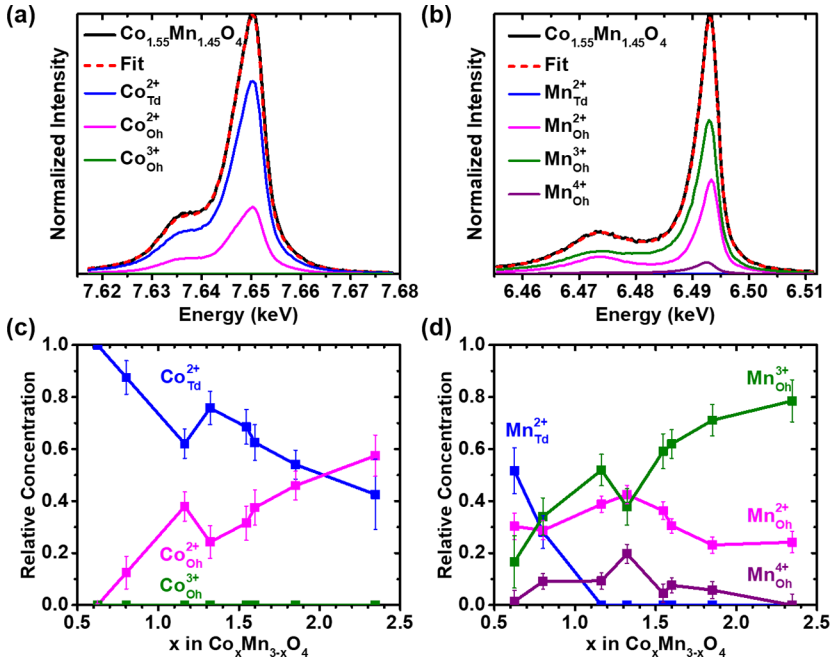

Figure 2. Spin, oxidation state, and ligand sensitive K$\beta_{1,3}$ (3p →1s) spectra are obtained using X-ray emission spectroscopy (XES) for different stoichiometries of $Co_xMn_{3-x}O_4$ NPs. The figure shows the XES spectra and the fitting of the model system $Co_{1.55}Mn_{1.45}O_4$ NPs for (a) Co−Kβ peak and (b) Mn−Kβ peak. K$\beta_{1,3}$ peak is observed at higher emission energies and the satellite Kβ' peak at lower emission energies. Superscripts represent the oxidation state, and subscripts represent the ligand geometry of cations. (c, d) Relative concentration of different cation species for (c) Co cations and (d) Mn cations. Co atoms are present only as 2+ oxidation state at both tetrahedral (T_d) and octahedral (O_h) sites, while Mn atoms are present as 2+ at T_d sites, and as 2+, 3+, and 4+ at O_h sites. Note: The contribution of CoO is excluded in (c).

spinel phase, and the value of x and y are determined from XES analysis.

XES is used to quantify the site occupation concentration of the cations, including information on the oxidation state, spin state, ligand geometry, and ligand identity (Figure 2a,b).[10−14] We previously showed that XES can accurately quantify the concentration of different cation species with average error of 3.5%; thus, it considerably outperforms the more widely used X-ray absorption spectroscopy (XAS), which has an average error of 16%.[10] In particular, we are interested in cation identities at the octahedral [O_h] sites, because the O_h sites are thought to be the pathway for polaron hopping.[3,5] In our $Co_xMn_{3-x}O_4$ NPs, two species of Co are observed, Co^{2+}_{Td} and Co^{2+}_{Oh}, where the superscripts (2+) represent the oxidation state, and subscripts (T_d and O_h) represent the ligand geometry of cations. The Co^{2+}_{Oh} species present in both the CoO impurity and the spinel phase must necessarily be deconvolved to gain insight into the spinel arrangements (Table S2). The cation site occupation is processing dependent, so unlike previous studies,[1,4] no Co^{3+}_{Oh} species is observed in our samples. On this basis, we attribute the absence of Co^{3+}_{Oh} and the presence of Mn^{4+}_{Oh} in our samples to charge balancing at the O_h sites. Overall, as the Co content increases, the concentration of Co atoms present at T_d sites, i.e., Co^{2+}_{Td}, decreases, whereas the concentration of Co atoms present at O_h sites, i.e., Co^{2+}_{Oh}, increases (Figure 2c). For Mn, four different species are observed − Mn^{2+}_{Td}, Mn^{2+}_{Oh}, Mn^{3+}_{Oh}, and Mn^{4+}_{Oh} (Figure 2d). We find that the T_d sites only have 2+ oxidation state cations of Mn and Co, whereas cations on O_h sites adopt mixed oxidation states, as expected for $Co_xMn_{3-x}O_4$ systems.[1,4] For $x \geq 1.16$ samples, no Mn atoms are present at T_d sites, and O_h sites are occupied by both Co and Mn atoms. The relative concentration of Mn^{2+}_{Td} decreases with increasing x, and for $x \geq 1.16$, no such species is present. With increasing x, the relative concentrations of Mn^{2+}_{Oh} and Mn^{4+}_{Oh} both show a maximum at $x = 1.32$. Overall, the relative concentration of both Mn^{2+}_{Oh} and Mn^{4+}_{Oh} varies by ∼20% as a function of stoichiometry x. For the Mn^{3+}_{Oh} species, an increasing concentration with x is observed with an overall change of 60% over our stoichiometric range.

To determine the complex electronic conductivity, activation energies for charge transport, and, by extension, the hopping mechanisms, dielectric impedance measurements[15−20] at different temperatures are carried out. This method is chosen over conventional transport measurement techniques as it is suitable for extracting the intrinsic electronic conductivity of the nanoparticles by modeling and removing the contributions to conductivity from grain boundaries (GBs) (see SI for details).[16,17] The packing density for all samples are kept constant to avoid the role of packing fraction and grain interfaces in influencing the electronic conductivity. The dielectric measurements are expressed as Nyquist plots (Figure 3a,b and Figure S6), which are fitted using an equivalent circuit[17,20] (Figure 3c) to extract conductance values for intraparticle (IP, charge transfer within a NP grain) and GB (charge transfer between NPs) pathways for all stoichiometries in the temperature range of 373 to 548 K. Measurements of electronic conductivity are confined to the stoichiometries in the range of $x = 0.88$ to 1.84, beyond which the samples become highly resistive and show incomplete semicircles, thus limiting the quality of the fits used to extract the conductivity parameters. The electronic conductivity in noncrystalline semiconductor solids is typically driven by thermally activated small polaron hopping. $Co_xMn_{3-x}O_4$ is a p-type semiconductor,[1] and the general relation for conductivity is expressed as[21]

DOI: 10.1021/acs.chemmater.9b01198
Chem. Mater. 2019, 31, 4228−4233

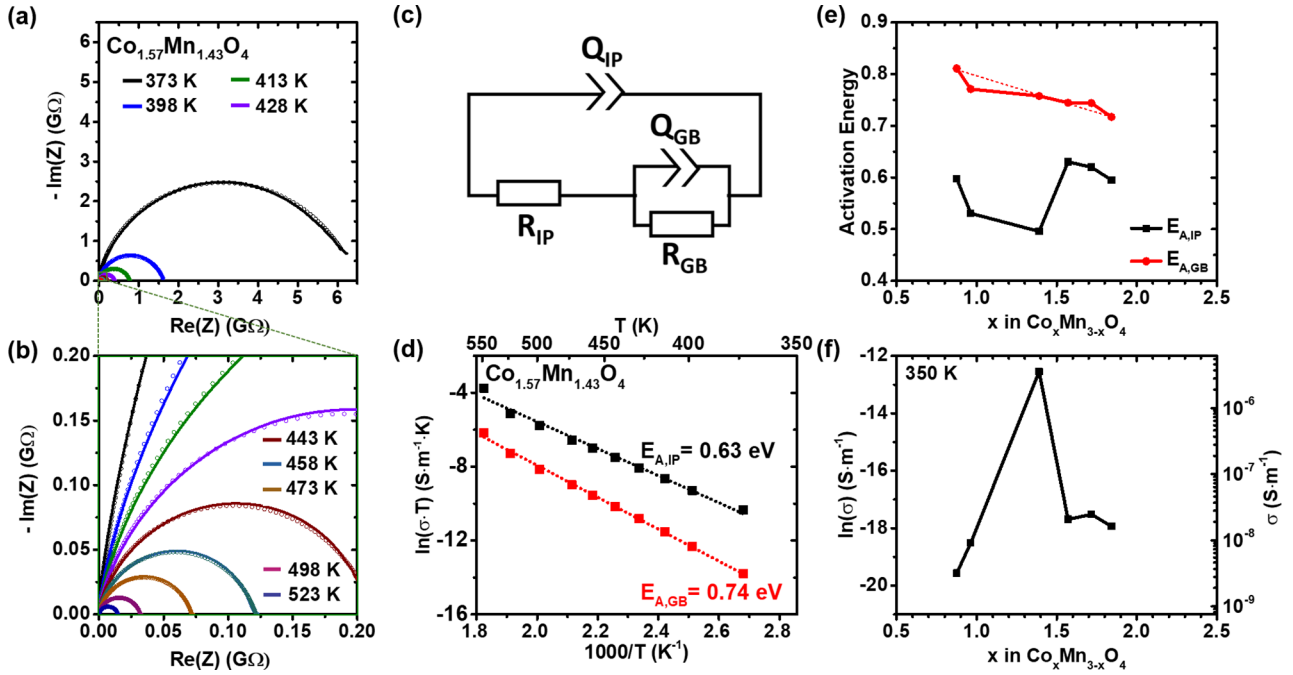

Figure 3. Dielectric spectroscopy measurements to determine the electronic conductivity, polaron hopping mechanism, and activation energies of $Co_xMn_{3-x}O_4$ NPs. (a) Nyquist plots for the model system $Co_{1.57}Mn_{1.43}O_4$ NPs. (b) Expanded view of the highlighted region (green box) of Nyquist plots in part (a) to show the impedance values at higher temperatures. (c) The equivalent circuit used in the fitting of the Nyquist plots (dotted lines) to extract the resistance values and to decouple the effects of the intraparticle (IP) and the grain boundary (GB) conductivities. A temperature series is used to extract the activation energies (E_A). (d) Arrhenius plot of the extracted conductivity values versus the inverse of temperature. (e) Variation of extracted E_A values as a function of x. (f) Variation of intraparticle conductivity (measured at 350 K) with change in x values.

$$\sigma(T) = \frac{C}{T^{\alpha}} \times \exp\left(\frac{-E_A}{k_B T}\right)^{P} \quad (1)$$

where σ is the electronic conductivity, C, α, and P are constants, k_B is the Boltzmann constant, T is the temperature, and E_A is the activation energy. The electronic conductivity plotted as a function of inverse of temperature shows a linear trend for all stoichiometries (Figure 3d shows a representative sample at $x = 1.57$). Least-squares fitting shows that $P = \alpha = 1$ for all stoichiometries, which implies the nearest neighbor hopping mechanism (NNH).[21] The GBs also follow the NNH mechanism, as has been previously shown for GBs in other spinel oxides.[16]

The E_A of the IP and GB hopping pathways ($E_{A,IP}$ and $E_{A,GB}$, respectively) are extracted by fitting the conductivity–temperature plots (Figure 3d and Figure S6). The GB activation energy follows a linear trend with stoichiometry and gradually decreases as the Co content increases (Figure 3e). $E_{A,IP}$ is much lower than $E_{A,GB}$, with the $E_{A,GB}$ up to twice as high as the $E_{A,IP}$ for certain stoichiometries. $E_{A,IP}$ varies in the range of 0.49 to 0.63 eV, consistent with previously reported values for bulk $Co_xMn_{3-x}O_4$.[4] With increasing Co content, the $E_{A,IP}$ initially decreases and then increases, with an inflection point around $x = 1.39$.[21,22] The origin of an inflection point in the activation energy at $x \approx 1.5$ has previously been explained by the change in the hopping distance between polaron hopping sites due to the phase change from tetragonal to cubic phase.[4]

The electronic conductivity measured at 350 K (Figure 3f) shows a large variation with stoichiometry. The highest electronic conductivity (3.55×10^{-6} S/m) is observed at $x = 1.39$, 3 orders of magnitude higher than in the least conductive sample (3.19×10^{-9} S/m for $x = 0.88$). Because the $Co_xMn_{3-x}O_4$ NPs are contaminated with CoO, we calculate the corrected electronic conductivity by taking into consideration the presence of insulating CoO particles. Corrections for the insulating impurity (CoO) result in negligible changes to conductivity trends in Figure 3f (Figure S7).

For NNH in the polaron model, the pre-exponential term in the electronic conductivity (eq 1) can be further expressed as[3]

$$\sigma_0 = \frac{gNc(1-c)e^2a^2\nu}{kT} \quad (2)$$

where g is the geometric factor, N is the density of charge carriers at O_h sites, and c is the cation donor ratio for cations of M [$c_M = M^{n+}/(M^{n+} + M^{(n+1)+})$], a is the hopping distance between donor/acceptor sites, e is the charge of electron, and ν is the lattice vibration frequency. Based on the temperature range for the electronic conductivity measurements, polaron hopping is considered to occur between O_h sites.[23] In the NNH model, the concentration of donor/acceptor hopping pairs, $c(1-c)$, is directly proportional to the electronic conductivity, and this is the dominant variable in the pre-exponential term. However, for a ternary system like $Co_xMn_{3-x}O_4$, the polaron hopping model does not identify the contribution of Co vs Mn hopping pairs (or mixtures) to the $c(1-c)$ term.

To determine the underlying mechanisms of charge transport, we first identify the identity of the active redox couples mediating polaron hopping and plot their concentration as a function of stoichiometry (Figure 4a). Because Co atoms are only present as 2+ oxidation state at O_h sites in our samples, there are no Co donor/acceptor hopping pairs, so we consider only the Mn pairs. We find that the concentration of

DOI: 10.1021/acs.chemmater.9b01198
Chem. Mater. 2019, 31, 4228–4233

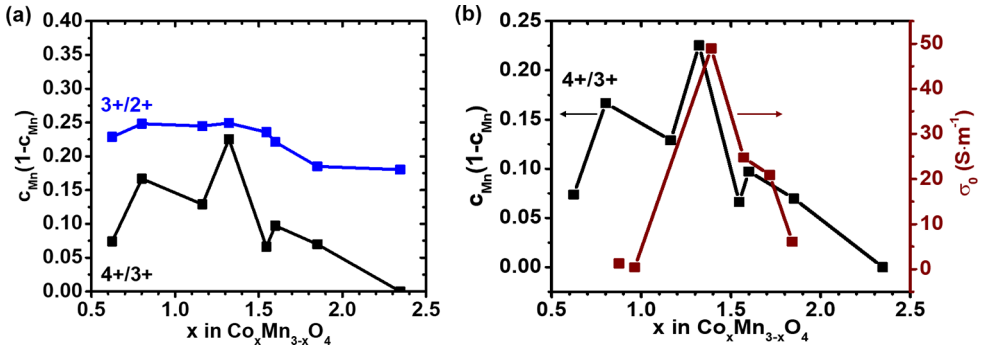

Figure 4. (a) Individual contributions of Mn^{3+}/Mn^{2+} and Mn^{4+}/Mn^{3+} hopping pairs to the total concentration of hopping pairs c(1 − c). The Mn^{3+}/Mn^{2+} pairs are relatively constant with stoichiometry, whereas the 4+/3+ pairs follow a volcano trend. (b) Comparison of donor/acceptor hopping pairs of Mn^{4+}/Mn^{3+} with the pre-exponential term of electronic conductivity. A positive correlation is observed, indicating Mn^{4+}/Mn^{3+} to be the active species.

Mn^{4+}/Mn^{3+} hopping pairs show a volcano trend as a function of stoichiometry, peaking at around x = 1.32, whereas the Mn^{3+}/Mn^{2+} hopping pairs remain relatively constant over the whole range. The x = 1.32 sample has the highest concentration of both the Mn^{3+}/Mn^{2+} and Mn^{4+}/Mn^{3+} hopping pairs with a value of 0.25 and 0.23, respectively (Figure 4a) (note: the maximum possible value of $c(1-c)$ is 0.25 when c = 0.5). The relatively constant concentration of Mn^{3+}/Mn^{2+} hopping pairs indicates that the stoichiometric-dependent behavior must be due to the Mn^{4+}/Mn^{3+} hopping pairs. Therefore, the site occupation of Mn cations at O_h sites can be plotted as the concentration of donor/acceptor hopping pairs $c_{Mn}(1-c_{Mn})$ (Figure 4b, black points) where c_{Mn} is the cation donor ratio of Mn^{4+}/Mn^{3+} pairs at O_h sites, i.e.,

$$c_{Mn}(1-c_{Mn}) = \frac{Mn^{3+}}{(Mn^{3+}+Mn^{4+})}\frac{Mn^{4+}}{(Mn^{3+}+Mn^{4+})} \quad (3)$$

A comparison of the trends in hopping pairs and electronic properties is shown in Figure 4b, where the pre-exponential term of the electronic conductivity, σ_0, is plotted on the right y-axis (brown points) and $c_{Mn}(1-c_{Mn})$ for the Mn^{4+}/Mn^{3+} hopping pairs on the left y-axis (black points). The concentration of donor/acceptor hopping pairs shows a direct correlation with the electronic conductivity, both peaking at the same stoichiometry. The minor offset between the two sets of data (0.07 on the x-axis) could be due to the different series of samples used for XES and dielectric spectroscopy. From this result, we find the trend for electronic conductivity correlates directly with the Mn^{4+}/Mn^{3+} hopping pairs, and we conclude that the Mn atoms are the only active species. Although Co atoms do not have hopping pairs, they still contribute to the performance of the $Co_xMn_{3-x}O_4$ system by modifying the concentrations of other species. Mn_3O_4 is a normal spinel, with only Mn^{3+} cations at O_h sites, and therefore lacks Mn^{4+}/Mn^{3+} hopping pairs. The introduction of Co to the system creates configurational disorder, leading to the generation of hopping pairs for Mn at O_h sites and, therefore, the increased electronic conductivity.

We investigate the effect of stoichiometry variations on the electronic structure of $Co_xMn_{3-x}O_4$ by calculating the projected density of states (PDOS) using hybrid density functional theory HSE06.[24] The spin-resolved PDOS plots (Figure S9) show a defect-like empty state within the band gap, as observed in other spinel systems.[25] The defect-like empty state lies just below the conduction band and moves to higher energies in end-point stoichiometries (Co- or Mn-rich), leading to more insulator-like behavior (larger band gap). Furthermore, these in-gap states at end-point geometries appear as sharp peaks in the PDOS and primarily arise from hybridization of the orbitals of one transition metal (Co or Mn), whereas at intermediate stoichiometries the density of the unoccupied states is less narrow and shows overlapping contributions to the PDOS from several different species. All of these are characteristic features of a more conductive material at intermediate stoichiometries. An increase in band conductivity at intermediate compositions aligns with our observed trends for the small polaron hopping model, confirming that there should be a synergistic increase in conductivity. However, the DFT results raise the concern that the polaron hopping model is oversimplified, and band transport could provide a pathway for electronic charge transfer that is not appreciated by the current polaron models.

In conclusion, for the spinel $Co_xMn_{3-x}O_4$ system, we determined the dominant performance parameter to be the concentration of Mn donor/acceptor hopping pairs. The site occupation of cations is determined using XES, and a stoichiometry-dependent concentration of different cation species is observed. The electronic property evaluation of $Co_xMn_{3-x}O_4$ NPs shows a volcano trend as a function of stoichiometry, with a peak performance around x = 1.39. Furthermore, 3 orders of magnitude change in electronic conductivity with stoichiometry is observed, showing that the site occupation of cations significantly affects the electronic conductivity. Finally, we demonstrate a positive correlation between these performance metrics and the concentration of Mn donor/acceptor hopping pairs, more specifically Mn^{4+}/Mn^{3+} hopping pairs. Ultimately, this work provides a starting point to formulate a more general theory of charge transport for all ternary and higher order spinels.

■ ASSOCIATED CONTENT

Supporting Information

The Supporting Information is available free of charge on the ACS Publications website at DOI: 10.1021/acs.chemmater.9b01198.

Experimental details and structural characterization using SXRD, XAS, and XES, electronic characterization using dielectric spectroscopy and projected density of states (PDF)

DOI: 10.1021/acs.chemmater.9b01198
Chem. Mater. 2019, 31, 4228−4233

AUTHOR INFORMATION

Corresponding Author

*E-mail: rdr82@cornell.edu.

ORCID

Anuj Bhargava: 0000-0002-5961-6171
Cindy Y. Chen: 0000-0003-1073-4852
Andrew Nelson: 0000-0002-2635-8612
Christopher J. Pollock: 0000-0001-5736-513X
Maytal Caspary Toroker: 0000-0003-1449-2977
Richard D. Robinson: 0000-0002-0385-2925

Notes

The authors declare no competing financial interest.

ACKNOWLEDGMENTS

This work was supported in part by the National Science Foundation (NSF) under award numbers DMR-1809429, CMMI-1344562, CHE-1507753, and DMR-1149036. This work made use of Cornell Centre for Materials Research (CCMR) and Cornell High Energy Synchrotron Source (CHESS) facilities and was funded in part by National Science Foundation under award numbers DMR-1719875 and DMR-1332208, respectively. This research was also supported by a grant from the United States-Israel Binational Science Foundation (BSF), Jerusalem, Israel, and the United States National Science Foundation (NSF).

REFERENCES

(1) Rousset, A.; Tenailleau, C.; Dufour, P.; Bordeneuve, H.; Pasquet, I.; Guillemet-Fritsch, S.; Poulain, V.; Schuurman, S. Electrical Properties of $Mn_{3-x}Co_xO_4$ ($0 \leq x \leq 3$) Ceramics: An Interesting System for Negative Temperature Coefficient Thermistors. *Int. J. Appl. Ceram. Technol.* **2013**, *10* (1), 175−185.

(2) Perera, S. D.; Ding, X.; Bhargava, A.; Hovden, R.; Nelson, A.; Kourkoutis, L. F.; Robinson, R. D. Enhanced Supercapacitor Performance for Equal Co−Mn Stoichiometry in Colloidal $Co_{3-x}Mn_xO_4$ Nanoparticles, in Additive-Free Electrodes. *Chem. Mater.* **2015**, *27* (23), 7861−7873.

(3) Huang, Z.; Zhou, W.; Ouyang, C.; Wu, J.; Zhang, F.; Huang, J.; Gao, Y.; Chu, J. High Performance of Mn-Co-Ni-O Spinel Nanofilms Sputtered from Acetate Precursors. *Sci. Rep.* **2015**, *5*, 10899.

(4) Brylewski, T.; Kucza, W.; Adamczyk, A.; Kruk, A.; Stygar, M.; Bobruk, M.; Dabrowa, J. Microstructure and Electrical Properties of $Mn_{1+x}Co_{2-x}O_4$ ($0 \leq x \leq 1.5$) Spinels Synthesized Using EDTA-Gel Processes. *Ceram. Int.* **2014**, *40* (9), 13873−13882.

(5) Wei, C.; Feng, Z.; Scherer, G. G.; Barber, J.; Shao-Horn, Y.; Xu, Z. J. Cations in Octahedral Sites: A Descriptor for Oxygen Electrocatalysis on Transition-Metal Spinels. *Adv. Mater.* **2017**, *29* (23), 1606800.

(6) Kong, H.; Li, X.; Xuan, L.; Zhang, T.; Wang, Z.; Zhang, S.; Hou, Y. Effects of Substitutional Doping on Structural, Electrical, and Optical Properties of Nickel Manganite $NiMn_2O_4$ Films. *Appl. Phys. A: Mater. Sci. Process.* **2019**, *125* (2), 93.

(7) Hu, L.; Zhong, H.; Zheng, X.; Huang, Y.; Zhang, P.; Chen, Q. $CoMn_2O_4$ Spinel Hierarchical Microspheres Assembled with Porous Nanosheets as Stable Anodes for Lithium-Ion Batteries. *Sci. Rep.* **2012**, *2*, 986.

(8) Liang, Y.; Wang, H.; Zhou, J.; Li, Y.; Wang, J.; Regier, T.; Dai, H. Covalent Hybrid of Spinel Manganese − Cobalt Oxide and Graphene as Advanced Oxygen Reduction Electrocatalysts. *J. Am. Chem. Soc.* **2012**, *134* (7), 3517−3523.

(9) Li, C.; Han, X.; Cheng, F.; Hu, Y.; Chen, C.; Chen, J. Phase and Composition Controllable Synthesis of Cobalt Manganese Spinel Nanoparticles towards Efficient Oxygen Electrocatalysis. *Nat. Commun.* **2015**, *6*, 7345.

(10) Bhargava, A.; Chen, C. Y.; Finkelstein, K. D.; Ward, M. J.; Robinson, R. D. X-Ray Emission Spectroscopy: An Effective Route to Extract Site Occupation of Cations. *Phys. Chem. Chem. Phys.* **2018**, *20* (46), 28990.

(11) Bordage, A.; Trannoy, V.; Proux, O.; Vitoux, H.; Moulin, R.; Bleuzen, A. In Situ Site-Selective Transition Metal K-Edge XAS: A Powerful Probe of the Transformation of Mixed-Valence Compounds. *Phys. Chem. Chem. Phys.* **2015**, *17* (26), 17260−17265.

(12) Kühn, T.-J.; Hormes, J.; Matoussevitch, N.; Bönnemann, H.; Glatzel, P. Site-Selective High-Resolution X-ray Absorption Spectroscopy and High-Resolution X-ray Emission Spectroscopy of Cobalt Nanoparticles. *Inorg. Chem.* **2014**, *53* (16), 8367−8375.

(13) Glatzel, P.; Jacquamet, L.; Bergmann, Y.; de Groot, F. M. F.; Cramer, S. P. Site Selective EXAFS in Mixed Valence Compounds Using High-Resolution Fluorescence Detection: A Study of Iron in Prussian Blue. *Inorg. Chem.* **2002**, *41* (12), 3121.

(14) Peng, G.; deGroot, F. M. F.; Haemaelaeinen, K.; Moore, J. A.; Wang, X.; Grush, M. M.; Hastings, J. B.; Siddons, D. P.; Armstrong, W. H. High-Resolution Manganese x-Ray Fluorescence Spectroscopy. Oxidation-State and Spin-State Sensitivity. *J. Am. Chem. Soc.* **1994**, *116* (7), 2914−2920.

(15) Veena Gopalan, E.; Malini, K. A.; Saravanan, S.; Sakthi Kumar, D.; Yoshida, Y.; Anantharaman, M. R. Evidence for Polaron Conduction in Nanostructured Manganese Ferrite. *J. Phys. D: Appl. Phys.* **2008**, *41* (18), 185005.

(16) He, L.; Ling, Z. Y. Electrical Conduction of Intrinsic Grain and Grain Boundary in Mn-Co-Ni-O Thin Film Thermistors: Grain Size Influence. *J. Appl. Phys.* **2011**, *110* (9), 093708.

(17) Ali, H.; Karim, S.; Rafiq, M. A.; Maaz, K.; Rahman, A. U.; Nisar, A.; Ahmad, M. Electrical Conduction Mechanism in ZnS Nanoparticles. *J. Alloys Compd.* **2014**, *612*, 64−68.

(18) Chen, Y.; Zhang, X. Y.; Vittoria, C.; Harris, V. G. Giant Magnetodielectric Effect and Magnetic Field Tunable Dielectric Resonance in Spinel MnZn Ferrite. *Appl. Phys. Lett.* **2009**, *94* (10), 102906.

(19) Ponpandian, N.; Balaya, P.; Narayanasamy, A. Electrical Conductivity and Dielectric Behaviour of Nanocrystalline $NiFe_2O_4$ Spinel. *J. Phys.: Condens. Matter* **2002**, *14*, 3221−3237.

(20) Kolekar, Y. D.; Sanchez, L. J.; Ramana, C. V. Dielectric Relaxations and Alternating Current Conductivity in Manganese Substituted Cobalt Ferrite. *J. Appl. Phys.* **2014**, *115* (14), 144106.

(21) Han, H.; Lee, J. S.; Ryu, J. H.; Kim, K. M.; Jones, J. L.; Lim, J.; Guillemet-Fritsch, S.; Lee, H. C.; Mhin, S. Effect of High Cobalt Concentration on Hopping Motion in Cobalt Manganese Spinel Oxide ($Co_xMn_{3-x}O_4$, $x \geq 2.3$). *J. Phys. Chem. C* **2016**, *120* (25), 13667−13674.

(22) Bordeneuve, H.; Tenailleau, C.; Guillemet-Fritsch, S.; Smith, R.; Suard, E.; Rousset, A. Structural Variations and Cation Distributions in $Mn_{3-x}Co_xO_4$($0 \leq x \leq 3$) Dense Ceramics Using Neutron Diffraction Data. *Solid State Sci.* **2010**, *12* (3), 379−386.

(23) Dieckmann, R.; Witt, C. A.; Mason, T. O. Defects and Cation Diffusion in Magnetite (V): Electrical Conduction, Cation Distribution and Point Defects in $Fe_{3-\delta}O_4$. *Berichte der Bunsengesellschaft für Phys. Chemie* **1983**, *87* (6), 495−503.

(24) Heyd, J.; Scuseria, G. E.; Ernzerhof, M. Hybrid Functionals Based on a Screened Coulomb Potential. *J. Chem. Phys.* **2003**, *118* (18), 8207−8215.

(25) Ndione, P. F.; Shi, Y.; Stevanovic, V.; Lany, S.; Zakutayev, A.; Parilla, P. A.; Perkins, J. D.; Berry, J. J.; Ginley, D. S.; Toney, M. F. Control of the Electrical Properties in Spinel Oxides by Manipulating the Cation Disorder. *Adv. Funct. Mater.* **2014**, *24* (5), 610−618.

DOI: 10.1021/acs.chemmater.9b01198
Chem. Mater. 2019, 31, 4228−4233